Submitted: 27 September, 2023 Accepted: 03 November, 2023 Published: 30 December, 2023 DOI:10.22514/jomh.2023.138

ORIGINAL RESEARCH

JOMH Journal of Men's Health

Value of dynamic contrast-enhanced MRI and DWI in diagnosis of prostate cancer and its pathological comparison

Yanyan Shen[1], Shiyong Wu[1,*]

[1]Department of Radiological, First affiliated Hospital of Huzhou University, 313000 Huzhou, Zhejiang, China

***Correspondence**
sywu7725@163.com
(Shiyong Wu)

Abstract

This study aims to assess the diagnostic utility of dynamic contrast-enhanced magnetic resonance imaging (DCE-MRI) and diffusion-weighted imaging (DWI) in the detection of prostate cancer (PCa) and to investigate the correlation between DCE-MRI signal intensity-time (SI-T) curve parameters and angiogenesis in cancerous lesions. A total of 56 PCa patients and 50 benign prostatic hyperplasia (BPH) patients were enrolled, and their DCE-MRI and DWI images before surgery were analyzed. We also examined the association between DCE-MRI SI-T curve parameters and vascular endothelial growth factor (VEGF) or microvessel density (MVD). In the early stage of DCE-MRI, both PCa and BPH lesions exhibited higher enhancement levels compared to the surrounding normal prostate tissue, and during delayed scanning, BPH lesions and adjacent normal prostate tissue demonstrated substantial enhancement with minimal distinction. Conversely, PCa lesions exhibited relatively low signal intensity changes, distinguishing them from the surrounding normal tissue. Most SI-T curve patterns for PCa patients exhibited ascending and descending profiles, whereas BPH patients predominantly exhibited plateau or ascending curves ($p < 0.05$). PCa patients had lower peak times, higher enhancement degrees and rates, and elevated VEGF positivity rates and MVD counts compared to BPH patients ($p < 0.05$). Correlation analysis revealed a negative correlation between peak times of SI-T curve parameters and VEGF and MVD expression levels, while enhancement degree and rate exhibited positive correlations with these parameters ($p < 0.05$). In DWI images, hyperplastic foci were primarily isointense or slightly hyperintense, while cancerous foci were predominantly markedly hyperintense. Higher b-values were associated with lower apparent diffusion coefficient (ADC) values. However, across various b-values, PCa consistently exhibited lower ADC values than BPH ($p < 0.05$). DCE-MRI and DWI are valuable tools for distinguishing between PCa and BPH.

Keywords

MRI; Dynamic enhancement; DWI; Prostatic carcinoma; Angiogenesis within cancer foci

1. Introduction

Prostate cancer (PCa) is a common malignancy among elderly men, often exhibiting clinical symptoms that closely resemble those of benign prostatic hyperplasia (BPH), which can lead to missed diagnosis [1–4]. Magnetic resonance imaging (MRI) has high soft tissue resolution and offers valuable insights for PCa diagnosis through multi-parameter imaging [5–7]. Notably, PCa tissue is characterized by an abundant vascular density, resulting in distinct differences in blood supply and vascularity compared to BPH and forms the basis for using dynamic contrast-enhanced MRI (DCE-MRI) in PCa diagnosis [8–10]. Diffusion-weighted MRI (DWI) can be used to assess the mobility of water molecules within tissues. Cancerous tissues usually disrupt the normal water-rich glandular structure, resulting in an increased nucleocytoplasmic ratio in tumor cells and structural remodeling, which impede the lateral molecular movement within cancerous lesions, thereby establishing a basis for distinguishing PCa using DWI [11–13].

Angiogenesis plays a pivotal role in the growth, metastasis, and invasion of malignant tumors. Vascular endothelial growth factor (VEGF) has emerged as a crucial regulatory factor in vascular processes, while microvessel density (MVD) remains the gold standard for assessing angiogenesis in tumors.

In this study, we examined the diagnostic potential of DCE-MRI and DWI for PCa and established a correlation between the signal intensity-time (SI-T) curve parameters obtained from DCE-MRI and angiogenesis in cancer foci.

Collectively, this research encompassed the application of MRI examination techniques, image analysis, diagnostic procedures, immunohistochemical examinations and rigorous statistical methodologies to shed light on the diagnostic utility of DCE-MRI and DWI-MRI in PCa.

2. Subjects and methods

In this study, we included a cohort of 56 patients diagnosed with PCa and 50 patients diagnosed with BPH who were admitted to our hospital between June 2020 and June 2022. The inclusion criteria comprised all patients who underwent thorough preoperative examinations, including DCE-MRI and DWI, with complete preoperative imaging data and pathological records. Exclusion criteria comprised individuals with known contrast medium allergies, those with cardiac pacemakers, and those presenting severe organ dysfunction involving critical organs such as the heart, liver or kidneys. The average ($\pm$standard deviation) age of the 56 PCa patients was 63.58 ($\pm$12.25) years (range: 54–81 years) and had an average weight of 73.15 ($\pm$13.15) kg (range: 61–84 kg). Among them, there were 12 stage I cases, 20 stage II PCa cases, 11 stage III PCa cases, 13 stage IV PCa cases, and 10 PCa cases with lymph node metastasis. According to the Gleason scoring system, 16 cases exhibited moderate differentiation, while 40 cases exhibited poor differentiation in PCa pathology. The average age of the 50 BPH patients was 64.07 ($\pm$10.78) years (range: 51–79 years) and their average weight was 74.52 ($\pm$12.37) kg (range: 60–84 kg).

3. Methods

3.1 MRI examination method

(1) The imaging equipment used in this study was the Philips Archieve 3.0T Tx superconducting magnetic resonance scanner (Philips, Amsterdam, Netherlands). The transmit coil employed was the body coil, while the receiving coil utilized was the 16-channel SENSE XL Torso coil. Contrast-enhanced scans were conducted using the Medrad Spectris Solaris automatic high-pressure injection system (USA).

(2) Before the examination, the patients were instructed to empty their bladders and assume a supine position in the scanning coil, aligning the pelvis accordingly. The midline of the coil was positioned to coincide with the midsagittal plane of the subject, and this midline was adjusted to align with the pubic symphysis. The imaging started with a T1-weighted imaging scan (Repetition Time (TR): 192 ms, Echo Time (TE): 10 ms), followed by a coronal slice-selective inversion recovery (SRIP) fat-suppressed T2-weighted imaging scan (TR: 1483 ms, TE: 70 ms, slice thickness: 5.0 mm, interslice distance: 1.0 mm, Field of View (FOV): 240 mm $\times$ 240 mm, matrix: 256 $\times$ 256).

(3) The DWI examination was performed utilizing a single-shot spin echo echo-planar imaging (EPI) sequence for transaxial scanning, which included the prostate gland and seminal vesicle, with b values set at 0, 500 and 100 s/mm^2. The scanning parameters were configured as follows: TR: 200 ms, TE: 58 ms, slice thickness: 3.0 mm, interslice distance: 1.0 mm, matrix: 256 $\times$ 256, FOV: 230 mm $\times$ 230 mm. Subsequently, the DWI scan data were transferred to the MR three-dimensional workstation, where software processing automatically generated apparent diffusion coefficient (ADC) maps.

(4) DCE-MRI examination was conducted using a 3D fast field echo sequence with transaxial scanning. Contrast medium Gd-DTPA was administered *via* a double-barrel high-pressure syringe through the cubital vein. The imaging started with an initial plain scan consisting of 8 phases, followed by the dynamic contrast-enhanced scan performed concurrently with the injection of the contrast medium, covering both the prostate and seminal vesicle. The specific imaging parameters included: TR (repetition time) of 5.5 ms, TE (echo time) of 1.7 ms, slice thickness of 6.0 mm, no interslice gap, FOV (field of view) measuring 230 mm $\times$ 230 mm, matrix dimensions of 256 $\times$ 256, and an inversion angle of 15°. Continuous scanning was performed over 96 phases, with each phase having a single-phase scanning time of 2.9 seconds. Subsequently, the DCE-MRI data was analyzed using the DCE@urLABv1.0 software package (Philips, Amsterdam, Netherlands). The right femoral artery was chosen to derive the arterial input function (AIF) curve model. Regions of interest (ROI) for cancerous and hyperplastic foci were manually delineated to construct the SI-T curves for recording important quantitative parameters, including peak time (Tmax), degree of enhancement (SIm%), and enhancement rate (R). Moreover, we categorized SI-T curves into ascending and descending types (indicating a signal decrease after early rapid enhancement), plateau type (characterized by a plateau after early rapid enhancement), and ascending type (exhibiting a relatively stable and gradual signal increase).

(5) The placement of ROI on both DCE and ADC maps was performed by experienced imaging experts according to a standardized procedure. T2 weighted imaging (T2WI) images were used as a reference for ROI placement, and the central level of the lesion was selected for ROI placement, where the ROI was oval-shaped, with an area controlled at approximately 0.4 cm^2. On ADC images, the ROI was positioned at the location corresponding to the lowest ADC value, while for DCE images, it was placed at the site showing early and pronounced enhancement within the lesion. Particular care was taken to avoid regions near the transitional zone-peripheral zone junction, the seminal vesicle root, blood vessels, and areas with hemorrhage or calcification.

3.2 Image analysis and diagnosis

Two MRI physicians assessed and summarized various aspects of the MRI scans, including the extent of lesion location, signal characteristics and patterns of enhancement in a double-blind manner, unaware of the results of the pathological diagnoses.

3.3 Prostate imaging reporting and data system version 2 (PI-RADSv2)

According to PI-RADSv2-related criteria, the probability of developing clinical PCa was assigned a score ranging from 1 point (indicating a very low likelihood of cancer) to 5 points

(indicating a very high likelihood of cancer) for categorization.

3.4 Immunohistochemical examination

PCa patients underwent radical prostatectomy, whereas those with BPH underwent transurethral resection. During the surgical procedures, tissue samples from the respective foci were collected, fixed using a 100 mL/L formalin solution and then embedded in conventional paraffin. Subsequently, 4 μm thick serial sections were prepared and subjected to hematoxylin and eosin (HE) staining. For immunohistochemical analysis, the Avidin Biotin–Peroxidase Complex technique (ABC) was employed. Specifically, 50 μL of diluted ready-to-use mouse anti-human VEGF polyclonal antibody or 50 μL of diluted ready-to-use mouse anti-human Cluster of Differentiation 34 (CD34) monoclonal antibody was added to each section. In the control group, phosphate-buffered saline (PBS) was used in place of the primary antibody to serve as a negative control. The experiment was performed using an immunohistochemical kit, and the associated reagents included mouse anti-human VEGF polyclonal antibody (Beijing Zhongshan Biotechnology Co., Ltd.) and mouse anti-human CD34 polyclonal antibody (Beijing Zhongshan Biotechnology Co., Ltd.).

The evaluation of VEGF expression involved the assessment of cells with brownish-yellow or brownish-yellow cytoplasm observed across the entire slide at low magnification ($\times$40). Three regions exhibiting the densest distribution of positive cells were identified. The quantification of positive and negative cells was conducted at high magnification ($\times$400) and categorized into four grades: absence of positive expression was denoted as negative ("–", 0 point), less than 25% positivity was labeled as low expression ("+", 1 point), positivity ranging from 25% to 50% was considered moderate expression ("++", 2 points), and greater than 50% positivity was designated as high expression ("+++", 3 points).

For the determination of vascular MVD, the protocol followed the guidelines established by Jiang *et al.* [14]. CD34 staining specifically targeted vascular endothelial cells, with brownish-yellow cells or cell plexus serving as indicators of blood vessels. Initially, the sections were examined under a light microscope at 100-fold magnification to identify the region exhibiting the highest concentration of blood vessels. Subsequently, the sections were further analyzed under a light microscope at 200-fold magnification to select the area with the densest presence of blood vessels for counting. The mean value of MVD was then computed based on these observations.

Gleason grading, based on criteria outlined by the International Society of Urology and Pathology (ISUP), was used to assess the PCa pathology. The Gleason score was determined as follows: Grade 1 ($\leq$6 points) represented well-defined neoplastic glands of moderate size with consistent sizes; Grade 2 (3 + 4 = 7 points) exhibited similarities to Grade 1 but with irregular nodule boundaries and possible mild glandular infiltration at the periphery; Grade 3 (4 + 3 = 7 points) featured tumor cells forming individual glands of varying sizes, smaller than Grades 1 and 2, with glandular lumens and neoplastic infiltration interspersed among normal glands; Grade 4 (4 + 4 = 8, 3 + 5 = 8, 5 + 3 = 8 points) involved fused glands with poorly defined or absent glandular lumens, often in cribriform or glomeruloid patterns; and Grade 5 (5 + 4 = 9, 4 + 5 = 9) displayed minimal glandular structures, single cells, cords or solid nests-like growth, sometimes accompanied by florid glandular structures, solid sheets, or comedo-necrosis. These grades were further categorized into two groups: high-grade (Gleason score $\geq$ 4 + 3 (7b)) and low-grade (Gleason score $\leq$ 3 + 7 (7a)).

3.5 Statistical methods

Data analysis was conducted using the SPSS 19.0 statistical software (BMI company, Chicago, IL, USA). Measurement data are presented as mean $\pm$ standard deviation ($\pm$s), and independent sample *t*-tests were utilized to compare the means between two groups. Enumeration data are presented as cases, and the χ^2 test was used to compare two groups. Pearson linear correlation analysis was applied to assess correlations between variables. Statistical significance was set at $p < 0.05$.

4. Results

4.1 DCE-MRI findings and quantitative analysis results of PCa and BPH

During the early phase of DCE MRI enhancement, there was a gradual enhancement observed in all cancerous lesions or hyperplastic nodules as the injection time progressed. Notably, the degree of enhancement in the lesions exceeded that observed in the surrounding normal prostate tissue. In the delayed scanning phase, the normal prostate tissue surrounding BPH nodules exhibited significant enhancement, making it challenging to differentiate from the lesion tissue. Conversely, in proximity to PCa tissue, the normal prostate tissue displayed pronounced enhancement, while the cancerous lesion tissue exhibited relatively reduced signal intensity changes. The results were presented in Fig. 1.

4.2 Comparison of SI-T curve type between PCa and BPH

The types of SI-T curves between PCa and BPH patients were compared, and the differences were found to be statistically significant ($p < 0.05$). This is shown in Table 1.

4.3 Comparison of SI-T curve parameters between PCa and BPH

The peak time of SI-T curve parameters in PCa patients was significantly lower than that in BPH patients ($p < 0.05$), and the enhancement degree and enhancement rate were higher than that in BPH patients ($p < 0.05$). This is shown in Table 2.

4.4 Comparison of VEGF and MVD detection results in PCa and BPH tissues

The positive rate of VEGF and MVD count in PCa tissues were higher than that in BPH, and the differences were statistically significant ($p < 0.05$). This is shown in Table 3.

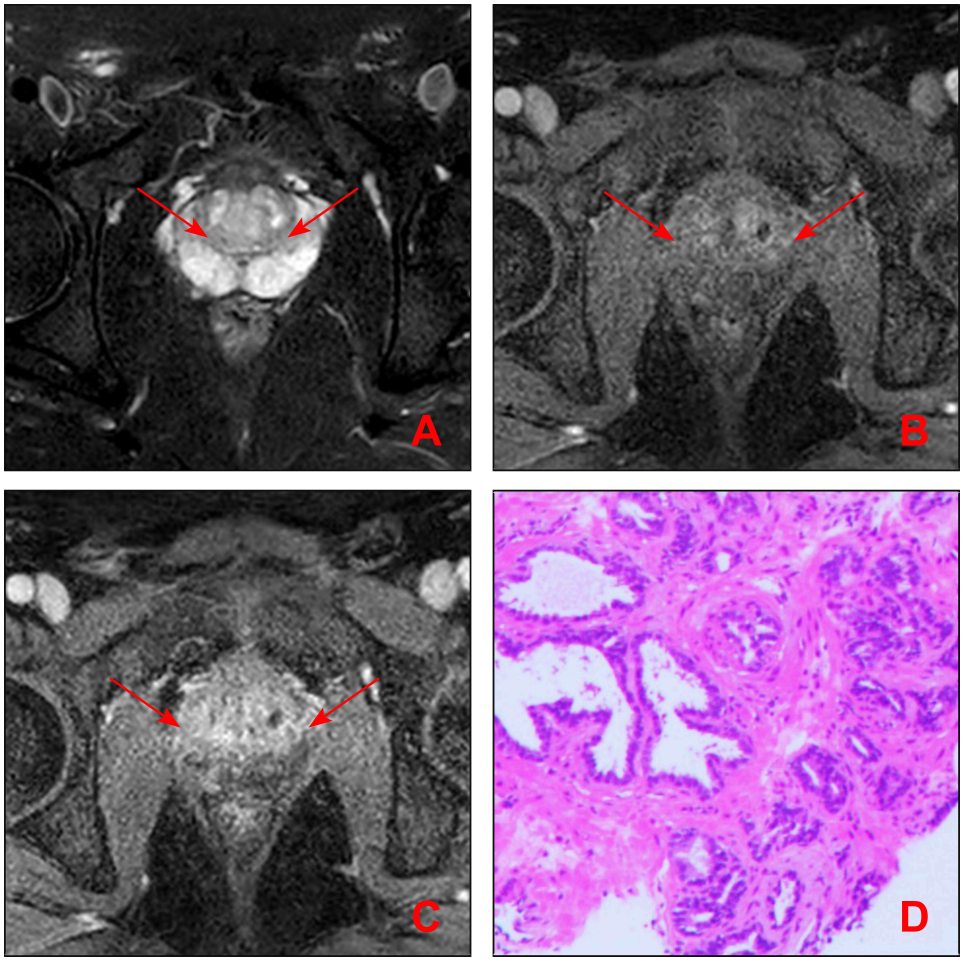

FIGURE 1. MRI images of a patient with benign prostatic hyperplasia. Note: Fig. 1 shows the MRI images of a 54-year-old male patient with benign prostatic hyperplasia. (A) T2WI images showing patchy hypointensity on both sides of the central gland (arrow); (B) early DCE MRI showing patchy hypointensity with enhancement; (C) delayed DCE MRI showing patchy enhancement without reduction (arrow). (D) Pathological confirmation of benign prostatic hyperplasia.

TABLE 1. Comparison of the SI-T curve type between PCa and BPH (n (%)).

Lesson type	n	Ascending and descending type	Plateau type	Ascending type
PCa	56	40 (71.43)	14 (25.00)	2 (3.57)
BPH	50	10 (20.00)	20 (40.00)	20 (40.00)
χ^2			33.554	
p			<0.001	

PCa: prostate cancer; BPH: benign prostatic hyperplasia.

TABLE 2. Comparison of SI-T curve parameters between PCa and BPH.

Lesion type	n	Peak time (Tmax)	Enhancement degree (SIm%)	Enhancement rate®
PCa	56	92.58 ± 16.58	235.15 ± 36.57	5.83 ± 1.54
BPH	50	173.99 ± 20.33	143.48 ± 29.64	2.98 ± 0.62
t		22.688	14.071	12.226
p		<0.001	<0.001	<0.001

PCa: prostate cancer; BPH: benign prostatic hyperplasia.

TABLE 3. Comparison of VEGF and MVD detection results in PCa and BPH tissues.

Group	n	VEGF (n (%))		MVD count
		Negative	Positive	
PCa	56	11 (19.64)	45 (80.36)	69.65 ± 12.58
BPH	50	39 (78.00)	11 (22.00)	22.34 ± 4.15
t/χ^2		36.099		25.377
p		<0.001		<0.001

VEGF: Vascular endothelial growth factor; MVD: microvessel density; PCa: prostate cancer; BPH: benign prostatic hyperplasia.

4.5 Relationship between SI-T curve parameters and VEGF or MVD expression levels in lesion tissues

The peak time of SI-T curve parameters was negatively correlated with VEGF and MVD expression levels, and the enhancement degree and enhancement rate were positively correlated with VEGF and MVD expression levels ($p < 0.05$). This is shown in Table 4.

TABLE 4. Relationship between SI-T curve parameters and VEGF or MVD expression levels in the lesion tissues.

SI-T parameters	VEGF	MVD
Peak time (Tmax)		
r	−0.522	−0.684
p	<0.001	<0.001
Enhancement degree (SIm%)		
r	0.411	0.553
p	<0.001	<0.001
Enhancement rate (R)		
r	0.537	0.771
p	<0.001	<0.001

SI-T: signal intensity-time; VEGF: Vascular endothelial growth factor; MVD: microvessel density.

4.6 DWI findings and quantitative analysis results of PCa and BPH

In DWI images, hyperplastic foci were primarily isointense or displayed slight hyperintensity, whereas cancerous foci were predominantly hyperintense. Notably, the ADC values associated with the foci decreased with increasing b values. However, across different b values, the ADC values of PCa were consistently lower than those of BPH, and this difference was statistically significant ($p < 0.05$). This is shown in Table 5.

4.7 Relationship between ADC value of lesions and VEGF and MVD expression levels in tissues

There was no significant correlation between ADC value and VEGF and MVD expression levels in the lesions ($p > 0.05$). This is shown in Table 6.

TABLE 5. Comparison of ADC values at different b-values between PCa and BPH ($\times 10^{-3}$ mm^2/s).

Lesion type	n	b = 500 s/mm^2	b = 1000 s/mm^2
PCa	56	0.74 ± 0.25	0.63 ± 0.16
BPH	50	1.26 ± 0.31	1.12 ± 0.21
t		9.549	13.595
p		<0.001	<0.001

PCa: prostate cancer; BPH: benign prostatic hyperplasia.

TABLE 6. Relationship between ADC value of lesions and expression levels of VEGF and MVD in tissues.

Parameters		VEGF	MVD
ADC value	r	0.156	0.143
	p	0.687	0.693

PCa: prostate cancer; BPH: benign prostatic hyperplasia; ADC: apparent diffusion coefficient.

4.8 Comparison of PI-RADSv2 Scores between PCa and BPH Lesions

The PI-RADSv2 value of PCa lesions was higher than that of BPH lesions, and the difference was statistically significant ($p < 0.05$). This is shown in Table 7.

TABLE 7. Comparison of PI-RADSv2 scores between PCa and BPH lesions.

Lesion type	n	PI-RADSv2
PCa	56	4.43 ± 0.74
BPH	50	3.02 ± 0.63
t		10.497
p		<0.001

PCa: prostate cancer; BPH: benign prostatic hyperplasia.

4.9 Comparison of PI-RADSv2 scores between high-grade and low-grade PCa tissues

Patients with high-grade lesions had significantly higher PI-RADSv2 scores than those with low-grade lesions ($p < 0.05$). This is shown in Table 8.

TABLE 8. Comparison of PI-RADSv2 scores between high-grade and low-grade PCa tissues.

Lesion	n	PI-RADSv2
Low-grade	20	3.74 ± 0.63
High-grade	36	4.63 ± 0.75
t		4.494
p		<0.001

4.10 Comparison of the value of PI-RADSv2 score in differentiating PCa from BPH

The ROC curve revealed that the PI-RADSv2 score had the highest value in differentiating PCa from BPH with 4 points as the cut-off line, and its diagnostic sensitivity, specificity and accuracy were 87.50%, 90.00% and 88.68%, respectively. This is shown in Table 9.

5. Discussion

Prior research has suggested that PCa tissue exhibits a twofold increase in vascular density compared to normal prostate tissue, with a more uniform vascular distribution [15]. In contrast, BPH tissue also experiences increased vascular density, but its distribution tends to be heterogeneous due to varying proportions of glands, stroma and smooth muscle [16]. In the present study, it was observed that during the early phase of DCE MRI, both PCa and BPH lesions gradually enhanced as the contrast agent circulated. The degree of enhancement within the lesion site exceeded that observed in the surrounding normal prostate tissue. However, in the delayed scanning phase, the normal prostate tissue surrounding BPH lesions exhibited noticeable enhancement, making it difficult to distinguish from the lesion tissue. Conversely, in proximity to PCa tissue, the normal prostate tissue displayed significant enhancement, while the cancerous lesion tissue exhibited relatively reduced signal intensity changes. SI-T curves were used to visualize the changes in signal intensity over time in DCE MRI, facilitating the quantification of blood supply to the lesion tissue, which provided more precise information during lesion enhancement [17–20]. In this study, 71.43% of 56 PCa patients were ascending and descending type, while SI-T curves of BPH patients were mostly plateau and ascending type. This observation could be associated with abundant microvessels in PCa tissue, high permeability of the microvascular system and a discontinuous basement membrane in new capillaries, allowing numerous contrast mediums to enter tumor tissue quickly [21–23]. Additionally, the peak time of SI-T curve parameters in PCa patients was lower than that in BPH patients, while the enhancement degree and rate were higher in PCa patients compared to those with BPH. Overall, these findings provide valuable insights for the diagnosis of both PCa and BPH.

Angiogenesis plays a pivotal role in the growth, metastasis, and invasion of malignant tumors, distinct from its manifestation in benign lesions [24–26]. Among them, VEGF is a crucial regulatory factor in vascular biology, contributing to tumor neovascularization and increased vascular permeability [27, 28]. MVD is the gold standard for assessing angiogenesis in tumors. In this study, we observed a higher positive expression rate of VEGF and increased MVD counts in PCa tissues compared to BPH tissues. Correlation analysis revealed a negative association between the expression levels of VEGF and MVD in the lesion tissues and the peak time of SI-T curve parameters, while a positive correlation was noted with the enhancement degree and rate. Specifically, the peak time reflects the speed of contrast medium infiltration into the lesion, while the enhancement intensity and rate signify the quantity of contrast medium entering the lesion. These findings highlight the important use of SI-T curves in delineating variations in vascular microcirculation between PCa and BPH.

In DWI scans, hyperplastic lesions were primarily characterized by isointensity or slight hyperintensity, while cancerous lesions exhibited a notably hyperintense appearance. When examining ADC values at the same b value, we observed that the ADC values in PCa patients were lower than those observed in tissues affected by BPH. The rationale behind this difference can be elucidated as follows: BPH tissues are characterized by the presence of abundant glandular and glandular duct tissues within the peripheral zone of the prostate, resulting in a significant extracellular space and enhanced mobility of water molecules. Consequently, these conditions contribute to higher ADC values [29–31]. Conversely, PCa tissues disrupt the normal water-rich glandular structures, replacing them with a limited amount of cellular stroma and densely packed, disorganized glandular structures, thereby constraining the movement of water molecules and leading to reduced ADC values. The b value represents the diffusion sensitivity coefficient, providing a measure of the extent of diffusion weighting. The DWI signal intensity comprises two key factors: spin-spin transverse relaxation (T2) and diffusion. Consequently, smaller b values exert a limited influence on the signal, resulting in weaker diffusion effects and images that closely resemble T2WI. Conversely, larger b values represent a higher degree of diffusion weighting, producing stronger gradient field strengths and increased sensitivity to diffusion. However, this may also lead to increased signal attenuation, potentially causing image distortion and blurring. The ADC value is expressed as ADC = Ln (Sz/Si)/(b2 − b1), where b represents values of 500 s/mm^2 and 1000 s/mm^2, and b1 equals 0 s/mm^2. This formula can also be condensed as ADC = Ln (S/So) b, with S representing the signal intensity obtained from the matrix image at the given b value and so indicating the signal intensity at the same matrix coordinate position when the b value is 0. Notably, as the b value increases, the image signal attenuation becomes more significant. This formula indicates that the measured ADC values tend to decrease as the b value increases.

The PI-RADSv2 system is used to assess the performance of various MRI scanning sequences and requires the use of multi-parameter and multi-sequence scans, including T2WI, DWI and DCE-MRI, as quantitative methods for evaluating lesion malignancy. In this present study, we observed that PI-RADSv2 scores were significantly higher in PCa patients than in those with BPH. Moreover, PI-RADSv2 scores were significantly increased in high-grade PCa cases compared to those with low-grade lesions. The sensitivity, specificity and

TABLE 9. Comparison of PI-RADSv2 score in differentiating PCa from BPH.

PI-RADSv2	Pathological diagnosis		Total	Sensitivity	Specificity	Accuracy
	PCa	BPH				
Malignant	49	5	54	87.50%	90.00%	88.68%
Benign	7	45	52			
Total	56	50	106			

PCa: prostate cancer; BPH: benign prostatic hyperplasia.

accuracy of PI-RADSv2 in differentiating between PCa and BPH were 87.50%, 90.00% and 88.68%, respectively.

6. Conclusions

Nonetheless, it is important to acknowledge the limitations of this study, including its relatively small sample size and being performed at a single institution. To enhance the robustness and generalizability of our study findings, we recommend conducting a large-scale, multicenter investigation. In summary, both DCE MRI and DWI demonstrate significant utility in distinguishing between PCa and BPH, with the SI-T curve parameters of DCE MRI serving as valuable indicators of angiogenesis status.

AVAILABILITY OF DATA AND MATERIALS

The authors declare that all data supporting the findings of this study are available within the paper and any raw data can be obtained from the corresponding author upon request.

AUTHOR CONTRIBUTIONS

YYS and SYW—designed the study and carried them out; supervised the data collection, analyzed the data, interpreted the data, prepared the manuscript for publication and reviewed the draft of the manuscript. All authors have read and approved the manuscript.

ETHICS APPROVAL AND CONSENT TO PARTICIPATE

Ethical approval was obtained from the Ethics Committee of First Affiliated Hospital of Huzhou University (Approval no 2020-029). Written informed consent was obtained from a legally authorized representative for anonymized patient information to be published in this article.

ACKNOWLEDGMENT

Not applicable.

FUNDING

This research received no external funding.

CONFLICT OF INTEREST

The authors declare no conflict of interest.

REFERENCES

[1] Monni F, Fontanella P, Grasso A, Wiklund P, Ou Y, Randazzo M, *et al*. Magnetic resonance imaging in prostate cancer detection and management: a systematic review. Minerva Urology and Nephrology. 2017; 69: 567–578.

[2] Panebianco V, Villeirs G, Weinreb JC, Turkbey BI, Margolis DJ, Richenberg J, *et al*. Prostate magnetic resonance imaging for local recurrence reporting (PI-RR): international consensus-based guidelines on multiparametric magnetic resonance imaging for prostate cancer recurrence after radiation therapy and radical prostatectomy. European Urology Oncology. 2021; 4: 868–876.

[3] O'Connor L, Wang A, Walker SM, Yerram N, Pinto PA, Turkbey B. Use of multiparametric magnetic resonance imaging (mpMRI) in localized prostate cancer. Expert Review of Medical Devices. 2020; 17: 435–442.

[4] Yoshida S, Takahara T, Arita Y, Sakaino S, Katahira K, Fujii Y. Whole-body diffusion-weighted magnetic resonance imaging: diagnosis and follow up of prostate cancer and beyond. International Journal of Urology. 2021; 28: 502–513.

[5] Stempel CV, Dickinson L, Pendsé D. MRI in the management of prostate cancer. Seminars in Ultrasound, CT and MRI. 2020; 41: 366–372.

[6] Emmett L, Buteau J, Papa N, Moon D, Thompson J, Roberts MJ, *et al*. The additive diagnostic value of prostate-specific membrane antigen positron emission tomography computed tomography to multiparametric magnetic resonance imaging triage in the diagnosis of prostate cancer (PRIMARY): a prospective multicentre study. European Urology. 2021; 80: 682–689.

[7] Bangma CH, van Leenders GJLH, Roobol MJ, Schoots IG. Restricting false-positive magnetic resonance imaging scans to reduce overdiagnosis of prostate cancer. European Urology. 2021; 79: 30–32.

[8] Fernandes CD, Mischi M, Wijkstra H, Barentsz JO, Heijmink SWTPJ, Turco S. Radiomic combination of spatial and temporal features extracted from DCE-MRI for prostate cancer detection. Annual International Conference of the IEEE Engineering in Medicine & Biology Society. 2021; 2021: 3153–3156.

[9] Huebner NA, Korn S, Resch I, Grubmüller B, Gross T, Gale R, *et al*. Visibility of significant prostate cancer on multiparametric magnetic resonance imaging (MRI)—do we still need contrast media? European Radiology. 2021; 31: 3754–3764.

[10] Breit HC, Block TK, Winkel DJ, Gehweiler JE, Glessgen CG, Seifert H, *et al*. Revisiting DCE-MRI. Investigative Radiology. 2021; 56: 553–562.

[11] Nakanishi K, Tanaka J, Nakaya Y, Maeda N, Sakamoto A, Nakayama A, *et al*. Whole-body MRI: detecting bone metastases from prostate cancer. Japanese Journal of Radiology. 2022; 40: 229–244.

[12] Hectors SJ, Said D, Gnerre J, Tewari A, Taouli B. Luminal water imaging: comparison with diffusion-weighted imaging (DWI) and PI-RADS for characterization of prostate cancer aggressiveness. Journal of Magnetic Resonance Imaging. 2020; 52: 271–279.

[13] De Perrot T, Sadjo Zoua C, Glessgen CG, Botsikas D, Berchtold L, Salomir R, *et al*. Diffusion-weighted MRI in the genitourinary system. Journal of Clinical Medicine. 2022; 11: 1921.

[14] Jiang J, Li J, Xiong X, Zhang S, Tan D, Yang L, *et al*. Different predictive values of microvessel density for biochemical recurrence among different PCa populations: a systematic review and meta-analysis. Cancer Medicine. 2023; 12: 2166–2178.

[15] Malyarenko DI, Swanson SD, McGarry SD, LaViolette PS, Chenevert TL. The impeded diffusion fraction quantitative imaging assay demonstrated in multi-exponential diffusion phantom and prostate cancer. Magnetic Resonance in Medicine. 2022; 87: 2053–2062.

[16] Dorairajan L, Dutt U, Kumar S, Badhe B, Manikandan R, Singh S. Effect of preoperative finasteride on perioperative blood loss during transurethral resection of the prostate and on microvessel density in patients with benign prostatic hyperplasia: an open label randomized controlled trial. Urology Annals. 2021; 13: 199.

[17] Li J, Ren Q, Shangguan J, Feng X, Ma X. Imaging features of dermatofibrosarcoma protuberans. Journal of Cancer Research and Therapeutics. 2022; 18: 476.

[18] Ziayee F, Mueller-Lutz A, Gross J, Ullrich T, Quentin M, Arsov C, *et al*. Arterial input function for quantitative dynamic contrast-enhanced MRI to diagnose prostate cancer. Diagnostic and Interventional Radiology. 2022; 28: 108–114.

[19] Abreu-Gomez J, Lim C, Cron GO, Krishna S, Sadoughi N, Schieda N. Pharmacokinetic modeling of dynamic contrast-enhanced (DCE)-MRI in PI-RADS category 3 peripheral zone lesions: preliminary study evaluating DCE-MRI as an imaging biomarker for detection of clinically significant prostate cancers. Abdominal Radiology. 2021; 46: 4370–4380.

[20] Akbari H, Kazerooni AF, Ware JB, Mamourian E, Anderson H, Guiry S, *et al*. Quantification of tumor microenvironment acidity in glioblastoma using principal component analysis of dynamic susceptibility contrast enhanced MR imaging. Scientific Reports. 2021; 11: 15011.

[21] Van Den Berghe T, Verstraete KL, Lecouvet FE, Lejoly M, Dutoit J. Review of diffusion-weighted imaging and dynamic contrast-enhanced MRI for multiple myeloma and its precursors (monoclonal gammopathy of undetermined significance and smouldering myeloma). Skeletal Radiology. 2022; 51: 101–122.

[22] Li Z, Xian M, Guo J, Wang CS, Zhang L, Xian J. Dynamic contrast-enhanced MRI can quantitatively identify malignant transformation of sinonasal inverted papilloma. The British Journal of Radiology. 2022; 95: 20211374.

[23] Yaligar J, Verma SK, Gopalan V, Anantharaj R, Thu Le GT, Kaur K, *et al*. Dynamic contrast-enhanced MRI of brown and beige adipose tissues. Magnetic Resonance in Medicine. 2020; 84: 384–395.

[24] Stocker D, Hectors S, Bane O, Vietti-Violi N, Said D, Kennedy P, *et al*. Dynamic contrast-enhanced MRI perfusion quantification in hepatocellular carcinoma: comparison of gadoxetate disodium and gadobenate dimeglumine. European Radiology. 2021; 31: 9306–9315.

[25] Coll-Font J, Afacan O, Chow JS, Lee RS, Warfield SK, Kurugol S. Modeling dynamic radial contrast enhanced MRI with linear time invariant systems for motion correction in quantitative assessment of kidney function. Medical Image Analysis. 2021; 67: 101880.

[26] Kong L, Qi R, Zhou G, Ding S. Correlation analysis of survivin, ING4, CXCL8 and VEGF expression in prostate cancer tissue. American Journal of Translational Research. 2021; 13: 13784–13790.

[27] Larsson P, Syed Khaja AS, Semenas J, Wang T, Sarwar M, Dizeyi N, *et al*. The functional interlink between AR and MMP9/VEGF signaling axis is mediated through PIP5K1α/pAKT in prostate cancer. International Journal of Cancer. 2020; 146: 1686–1699.

[28] Leis-Filho AF, Lainetti PD, Kobayashi PE, Palmieri C, Amorim RL, Fonseca-Alves CE. Expression and prognostic significance of vascular endothelial growth factor-a (VEGF-a) and its receptor in canine prostate cancer. The Prostate. 2021; 81: 1021–1031.

[29] Abdelmaksoud IR, Shalaby A, Mahmoud A, Elmogy M, Aboelfetouh A, Abou El-Ghar M, *et al*. Precise identification of prostate cancer from DWI using transfer learning. Sensors. 2021; 21: 3664.

[30] Yao W, Liu J, Zheng J, Lu P, Zou S, Xu Y. Study on diagnostic value of quantitative parameters of intravoxel incoherent motion diffusion-weighted imaging (IVIM-DWI) in prostate cancer. American Journal of Translational Research. 2021; 13: 3696–3702.

[31] Hammon M, Saake M, Laun FB, Heiss R, Seuss N, Janka R, *et al*. Improved visualization of prostate cancer using multichannel computed diffusion images: combining ADC and DWI. Diagnostics. 2022; 12: 1592.

How to cite this article: Yanyan Shen, Shiyong Wu. Value of dynamic contrast-enhanced MRI and DWI in diagnosis of prostate cancer and its pathological comparison. Journal of Men's Health. 2023; 19(12): 119-126. doi: 10.22514/jomh.2023.138.